Journal of Hydroscience and Hydraulic Engineering
Vol. 26, No.1 May, 2008, 113-127

NUMERICAL SIMULATION AND FACTOR ANALYSIS OF FLUSHING RIVER MOUTH BAR

By

Takuya SAKAWA

Alpha Hydraulic Engineering Consultants Co., Ltd (9-14-516-336 Hassamu, Nishi-ku Sapporo-shi, Hokkaido 063-0829, Japan)

Yasuro OHTANI

Alpha Hydraulic Engineering Consultants Co., Ltd. Tokyo Branch (4-15-35 Mita, Minato-ku Tokyo 103-0073, Japan)

Shingo ICHIKAWA

Alpha Hydraulic Engineering Consultants Co., Ltd (9-14-516-336 Hassamu, Nishi-ku Sapporo-shi, Hokkaido 063-0829, Japan)

Yoshinori TAKEUCHI

National Institute for Land and Infrastructure Management (1 Asahi Tsukuba-shi, Ibaraki 305-0804, Japan)

and

Takenori YAMASHITA

National Institute for Land and Infrastructure Management (1 Asahi Tsukuba-shi, Ibaraki 305-0804, Japan)

SYNOPSIS

A 2D river morphology model with a curvilinear grid is developed to simulate the flushing river mouth bar which occurred in the Ara River in July 2004. In the hydrodynamic model, the 2D free surface flow is calculated by Saint Venant equations which are solved by an implicit finite difference technique and the ADI method. In the morphological model, the Van Rijn's model is used to evaluate suspended and bed load sediment transport. The helical flow and the transverse bed slope modify the bed load sediment transport. The bed level change is computed by a sediment continuity equation with the bank erosion model. This model is validated by making a comparison with the observations of water level variations and the riverbed topography at the mouth. A factor analysis is conducted to evaluate the effects of discharge, tidal levels, and grain size. The result shows that the differences of sea elevation and peak discharge have significant effects on the process of morphological change at the river mouth.

INTRODUCTION

River mouth bars play an important role in flood control, water utilization and in the prevention of wave and salt-water intrusion. In general, it is flushed in major flooding event, however, it increases the risk of flooding due to rising of water levels at the upper reaches of the bar. For this reason, it is important for flood safety control to evaluate discharge capacity due to increase of flow area by erosion at river mouths during flushing events. Therefore, a quantitative evaluation for flushing river mouth bars is necessary for effective management of river mouth.

Many studies on 2D river morphology models of the flushing river mouth bars have been conducted since 1980's (for example, Sawaragei et al. (9), Kuwahara et al. (6) and Watanabe et al. (15)). In a recent study, a 2D river morphology model of the flushing river mouth bar at the Agano River was produced by Hosoyamada et al. (3), (4). However, this study did not take the bank erosion model into the account. On the other hand, Kawaguchi et al. (5) proposed a planning method for river mouth control by using a river morphology model with the slope failure effect. In addition, the effect of the flushing river mouth bar on water levels at the upper reaches is discussed by Takebayashi et al. (11).

In this study a 2D river morphology model with a curvilinear grid was developed and validated to simulate the flushing river mouth bar which occurred in the Ara River in July 2004. With the calibrated model a factor analysis was conducted to evaluate the effects of discharge, tidal levels, and grain size. All cases, including the calibration and the factor analysis, are listed in Table. 1.

Table. 1 Cases of the calibration and the factor analysis.

Case	Peak discharge (m^3/s)	Sea level (T.P.)	d_{50} (mm)	Remarks
Case-0	3,886	Observed at Iwafune Port (+0.6~0.9m)	2.0	Model calibration
Case-1	1,600	+0.34m (M.W.L)	2.0	Evaluation of the effects of discharge
Case-2	3,000			
Case-3	4,000			
Case-4	1,600	High tide at peak flow	2.0	Evaluation of the effects of tidal level
Case-5		Low tide at peak flow		
Case-6	4,000	High tide at peak flow		
Case-7		Low tide at peak flow		
Case-8	3,886	Observed at Iwafune Port (+0.6~0.9m)	0.5	Evaluation of the effects of grain size
Case-9			1.0	
Case-10			5.0	
Case-11			22.0	

AN OVERVIEW OF NUMERICAL MODEL

In the hydrodynamic model, the 2D surface flow is calculated by means of Saint Venant equations (1) based on vertical integrations of Navier-Stokes equations in a curvilinear coordinate system.

$$\frac{\partial H}{\partial t}+\frac{\partial p}{\partial s}+\frac{\partial q}{\partial n}-\frac{q}{R_s}+\frac{p}{R_n}=0 \qquad (1)$$

$$\frac{\partial p}{\partial t}+\frac{\partial}{\partial s}\left(\frac{p^2}{h}\right)+\frac{\partial}{\partial n}\left(\frac{pq}{h}\right)-2\frac{pq}{hR_n}+\frac{p^2-q^2}{hR_s}+gh\frac{\partial H}{\partial s}+\frac{gn^2p\sqrt{p^2+q^2}}{h^{5/3}}=RHS_s \tag{2}$$

$$\frac{\partial q}{\partial t}+\frac{\partial}{\partial s}\left(\frac{pq}{h}\right)+\frac{\partial}{\partial n}\left(\frac{q^2}{h}\right)+2\frac{pq}{hR_s}-\frac{q^2-p^2}{hR_n}+gh\frac{\partial H}{\partial n}+\frac{gn^2q\sqrt{p^2+q^2}}{h^{5/3}}=RHS_n \tag{3}$$

where s = the horizontal coordinate along the streamline; n = the horizontal coordinate in a transverse direction; p and q = the mass fluxes in the s- and n- direction; H = the water level; h = the water depth; g = the gravity acceleration; n = the Manning's roughness coefficient; R_s, R_n = the radius of curvature of s- and n-line; and RHS_s, RHS_n = the right hand side in the force balance in the s- and n- direction, which contains Reynolds stresses. The Reynolds stresses in the RHS term can be described in a curvilinear grid assuming a smooth grid (R_s and R_n are large and vary slowly:)

$$RHS_s=\frac{\partial}{\partial s}\left(h\cdot E\frac{\partial u}{\partial s}\right)+\frac{\partial}{\partial n}\left(h\cdot E\frac{\partial u}{\partial n}\right)-\frac{2hE}{R_s}\frac{\partial v}{\partial s}-\frac{\partial(h\cdot E)}{\partial s}\frac{v}{R_s}-\frac{2hE}{R_n}\frac{\partial v}{\partial n}-\frac{\partial(h\cdot E)}{\partial n}\frac{v}{R_n} \tag{4}$$

$$RHS_n=\frac{\partial}{\partial s}\left(h\cdot E\frac{\partial v}{\partial s}\right)+\frac{\partial}{\partial n}\left(h\cdot E\frac{\partial v}{\partial n}\right)+\frac{2hE}{R_s}\frac{\partial u}{\partial s}+\frac{\partial(h\cdot E)}{\partial s}\frac{u}{R_s}+\frac{2hE}{R_n}\frac{\partial u}{\partial n}+\frac{\partial(h\cdot E)}{\partial n}\frac{u}{R_n} \tag{5}$$

where E = the eddy viscosity, which is proportional to the velocity gradient in the Boussinesq hypothesis; and u, v = the velocity component in the curvilinear coordinate system. The equations are solved by an implicit finite difference technique with the ADI method.

In the morphological model, Van Rijn's model (13), (14) is adopted to evaluate sediment transport including bed load and suspended load. The bed load transport formula is defined as a function of a dimensionless particle parameter (D_*) and a transport stage parameter (T):

$$S_{bl}=0.053\frac{T^{2.1}}{D_*^{0.3}}\sqrt{(r-1)g\cdot d_{50}^{\ 3}} \tag{6}$$

where r = relative density of the sediment and d_{50} = median diameter of the sediment. T is defined as function of a bed shear velocity and a critical bed shear velocity. The bed load transport rate and its direction are corrected by the following equations to take into account the bed slope and helical flow effects (Olsen et al. (7), Talmon et al. (12)) :

$$S_{bs}=(1-\alpha\cdot\frac{\partial z}{\partial s})S_{bl} \tag{7}$$

$$S_{bn}=\left(\tan\delta_s-G\cdot\theta^{-\gamma}\cdot\frac{\partial z}{\partial n}\right)S_{bl} \tag{8}$$

where S_{bs}, S_{bn} = the bed transport rate in the s- and n- direction, respectively ; α = the correction coefficient for the bed slope effect; z = the bed level; G = the transverse bed slope factor; θ = the Shields parameter; γ = the transverse bed slope exponent; and $\tan\delta_s$ = the bed shear direction change due to helical flow strength. The bed shear direction change $\tan\delta_s$ for continuously varying curvature in steady flow conditions can be calculated by solving the transport equation (Struiksma et al. (10), Olsen et al. (7)).

$$\kappa_{sf}\frac{\partial(\tan\delta_s)}{\partial s}+\tan\delta_s=-\beta\cdot\frac{h}{R_s} \tag{9}$$

The parameter β is obtained by means of Rozovskii's logarithmic model (8). For the length scale for secondary flow adaptation κ_{sf}, the following differential length scale is applied:

$$\kappa_{sf}=\frac{1.2hC}{\sqrt{g}} \tag{10}$$

where C = Chezy number. On the other hand, the suspended load transport is calculated by the following equation:

$$S_{sl} = f \cdot c_a \cdot u \cdot h \tag{11}$$

where c_a = reference concentration ; and f = the correction factor for suspended load. An advection-dispersion model is applied to simulate the suspended sediment transport by convection and turbulent diffusion.

Based on the calculated suspended load and the bed load, the bed level changes are calculated from solving the sediment continuity equation:

$$(1-\lambda)\cdot\frac{\partial z}{\partial t}+\frac{\partial S_s}{\partial s}-\frac{S_n}{R_s}+\frac{\partial S_n}{\partial n}+\frac{S_s}{R_n}=\Delta S_e \tag{12}$$

where λ = the sediment porosity; S_s, S_n = the total sediment transport in the s- and n- direction, respectively; ΔS_e = the lateral sediment supply from bank erosion. In the bank erosion model bank erosion rate is expressed as a function of local bed level change and sediment transport just close to the bank (Enggrob et al. (2)):

$$E_b = -a\frac{\partial z}{\partial t}+b\frac{q_s}{h} \tag{13}$$

where a, b = calibration coefficient ; and q_s = near bank sediment transport. In this model the lateral erosion is translated directly into equivalent vertical bed level change in the following way (See Fig.1). The volume that is moved due to lateral erosion is calculated by:

$$V = E_b \Delta n \frac{\partial z}{\partial n}\Delta s \tag{14}$$

where Δs = the longitudinal length of the cell; Δn = the transverse length of the cell calibration coefficient. On the other hand, V is expressed as:

$$V = \Delta s \Delta n \Delta z \tag{15}$$

Thus, by equalizing these two expressions for the volume, the equivalent vertical bed level change becomes:

$$\Delta z_{eq} = E_b \frac{\partial z}{\partial n} \tag{16}$$

All parameters and calibration coefficients, which are applied in the hydrodynamic and morphological model, are listed in Table.2.

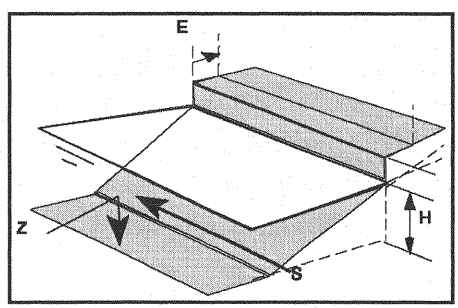

Fig. 1 Sketch of the bank erosion model.

Table. 2 Parameters and calibration coefficients applied in this model.

Name	Symbol	Value	Unit
Eddy viscosity	E	1.0	m^2/s
Bed transport model's parameters	α	5.0	-
	G	1.25	-
	γ	0.5	-
Bank erosion model's parameters	a	50.0	-
	b	40.0	-

AN OVERVIEW OF THE ARA RIVER

The Ara River originates in Daiasahidake in Yamagata Prefecture and flows in the northern part of Echigo Plain and flows into the Japan Sea at Arakawa Town in Niigata Prefecture (Fig.2). The river is about 73 km long from its headwaters and its watershed drains an area of approximately 1,150 km². In August 1967, a catastrophic flood, which was far larger than its design high water, occurred and took 90 lives. As a result, it was decided that it should be classified as a class A river and its design high water discharge was revised up to 6,500 m^3/s.

In 2004 heavy rain caused a large flood in the Ara River area from July 17th to 18th, and as a result most of the river mouth bar was flushed. A topographic change between pre- and post-flood is shown in Fig.2. The upper bathymetry in Fig.3 is based on a pre-flood surveys (Feb. 2004), and the lower one is based on post-flood surveys (July. 2004). The bar extended to a transversal direction, which is about 150m wide, and it almost blocked the flow of the river. After the flood, most of the bar was flushed, and shallow spots were left in the middle of the channel. In this study, we selected the flood event as a calibration case to develop the 2D river morphology model.

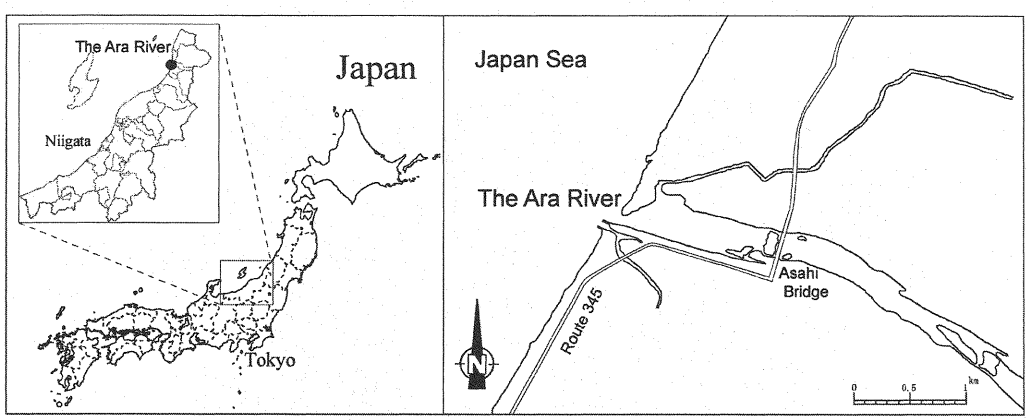

Fig. 2 Location of the river mouth at the Ara River.

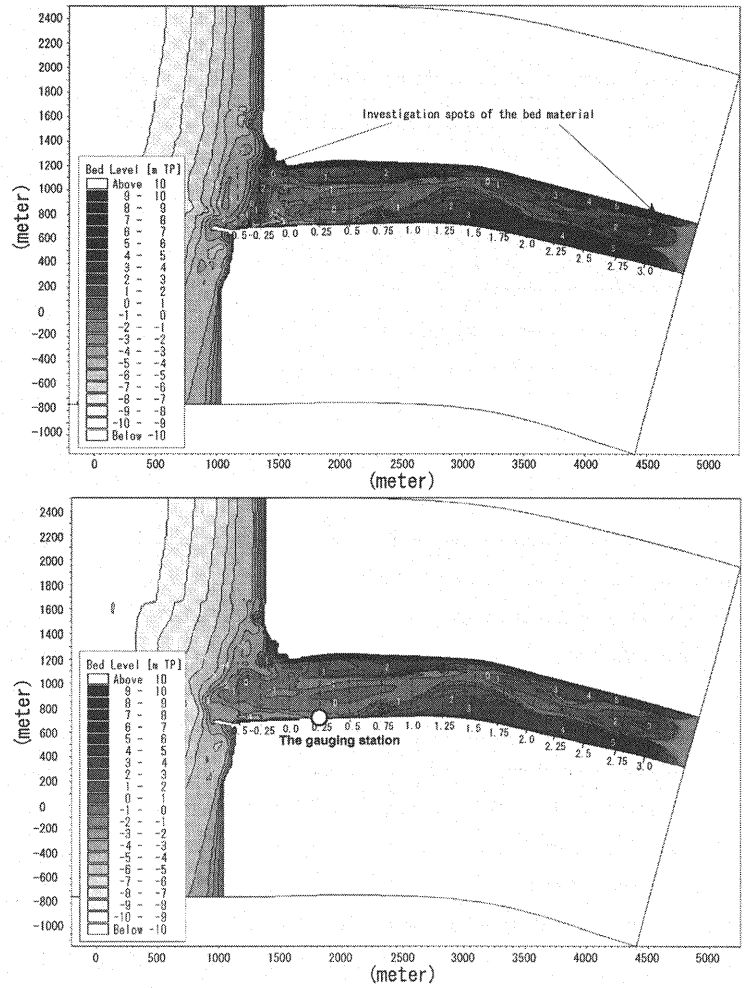

Fig. 3 Bathymetries based on pre-flood (upper) and post-flood (lower) surveys.

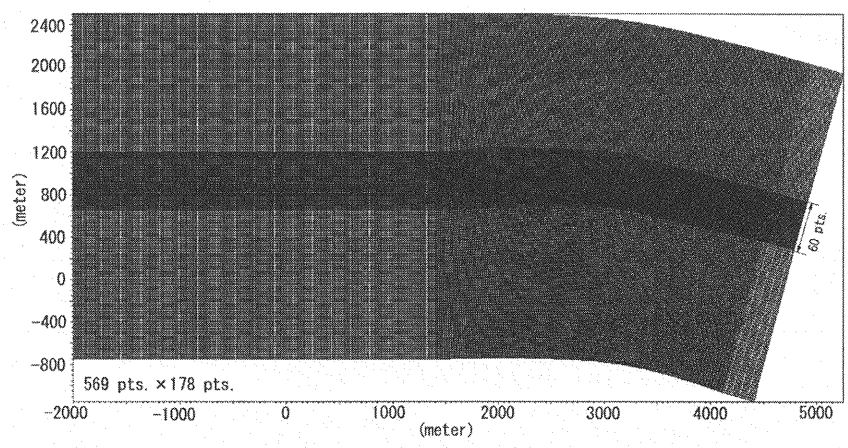

Fig. 4 Curvilinear grid of the river mouth at the Ara River.

CALIBRATION OF THE MODEL

The hydrodynamic model was calibrated and verified by simulating the observed water level during the flood period from 1 a.m. on July 17 to 0 a.m. on July 18 in 2004. The morphological model was also verified by making a comparison with a post-flood survey. The model consists of 596 by 178 curvilinear grid points and covers approximately 3.2km of the coast around the river mouth and 3 km of the channel (Fig.4). In consideration of the model stability, the time intervals in the hydrodynamic and morphological models were set to 2 and 6 seconds, respectively. In order to determine a representative grain size, several trials were conducted. As a result of these trials, the grain size was set to 2 mm and it corresponds to an averaged grain size of the bar and the upstream region (See Fig.5). Bed resistance is expressed by the Manning's roughness coefficient, which was set to 0.031 in the river channel and 0.045 in the flood plain, and the eddy viscosity was set to 1.0 m^2/s. The observed sea level at Iwafune Port was applied to the lower boundary condition, and the measured river discharge in Tsudurayama (4.6kp) was applied to the upper boundary condition.

Fig.6 shows a comparison of water level variations at the river mouth between the result of the simulation and the measurements. The simulated water level fluctuation and the peak level are in good agreement with the measurement. Therefore, the model is valid for a simulation of river mouth bar flushing in terms of the hydrodynamic aspect. On the other hand, a minor difference in water levels indicates a topographic discrepancy between the simulation and the measurement during the event. However, the simulated bed level after the flood (Fig.7) shows a close correlation with the survey (Fig.3) in terms of the geometry of the left bar and the topographic change in the upstream area of the bar. Although the erosion in the right side of the bar and the river mouth terrace are relatively underestimated, the model can simulate the bed level changes in the river mouth including the flushing mouth bar.

The simulated cross-sectional profile of the bar is plotted as Fig.8. The location of the profile is indicated as Line 1 in Fig.7. Compared with the post-flood survey, the location of erosion is similar to the observation, which indicates the validity of the model. On the other hand, the erosion is somewhat overestimated in the left hand side bar, while it is underestimated in the right hand side. There is a time lag between the event and the survey, which could account for the topographic discrepancy.

Fig.9 shows time variations of the cross-sectional profile of the water level and the bed level. When the discharge reached up to 2,000 m^3/s at 12 a.m. on 17th, the channels on both sides of the river mouth bar were subjected to erosion. Moreover, the water level rose enough to submerge the whole bar, and then the erosion began at the top of the bar. 2 hours later (at 14 p.m.), the discharge reached the peak flow (about 3,700 m^3/s) and a major part of the bar was flushed. The water level in the upper region of the bar continued rising up during the flood.

Finally, Fig.10 shows a distribution of calculated current speed at 12 p.m. (in the beginning of the flushing) and 16 p.m. (at the peak flow). In the beginning of the flushing, a strong current (over 3m/s) partially occurs in the channels beside the bar. On the other hand, a current speed exceeds about 3 m/s at the peak of discharge in the whole channel and the main flow is divided by the river mouth bar in the downstream.

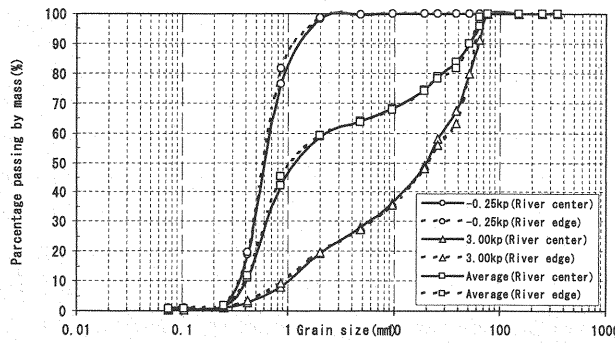

Fig. 5 Grain size distribution at the river mouth and the upstream region.

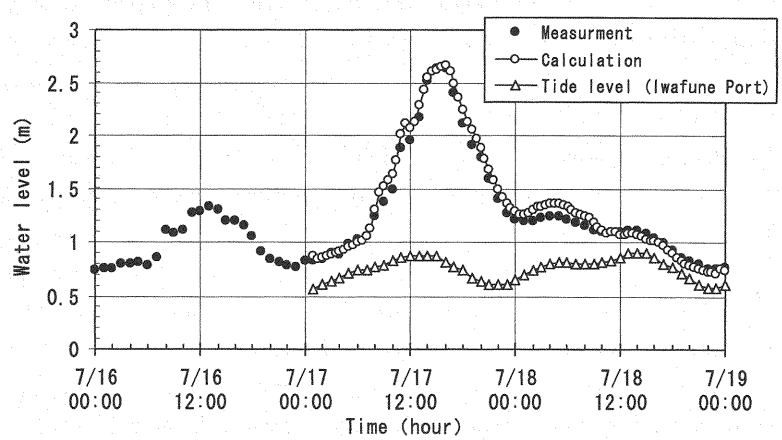

Fig. 6 Comparison of the water levels at the river mouth (See Fig.2) between the simulation and the measurement.

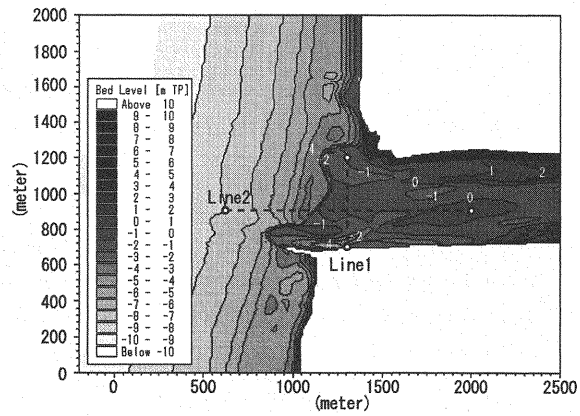

Fig. 7 Simulated bathymetry of the river mouth after the flood.

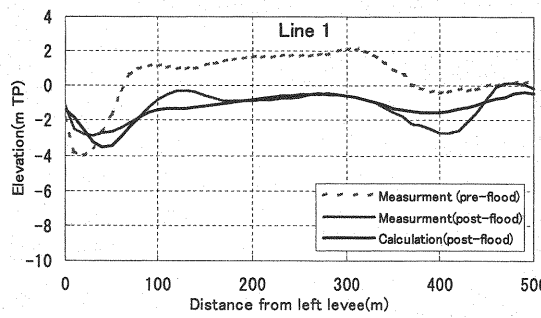

Fig. 8 Comparison of the cross sections at the bar between the simulation and the measurement.

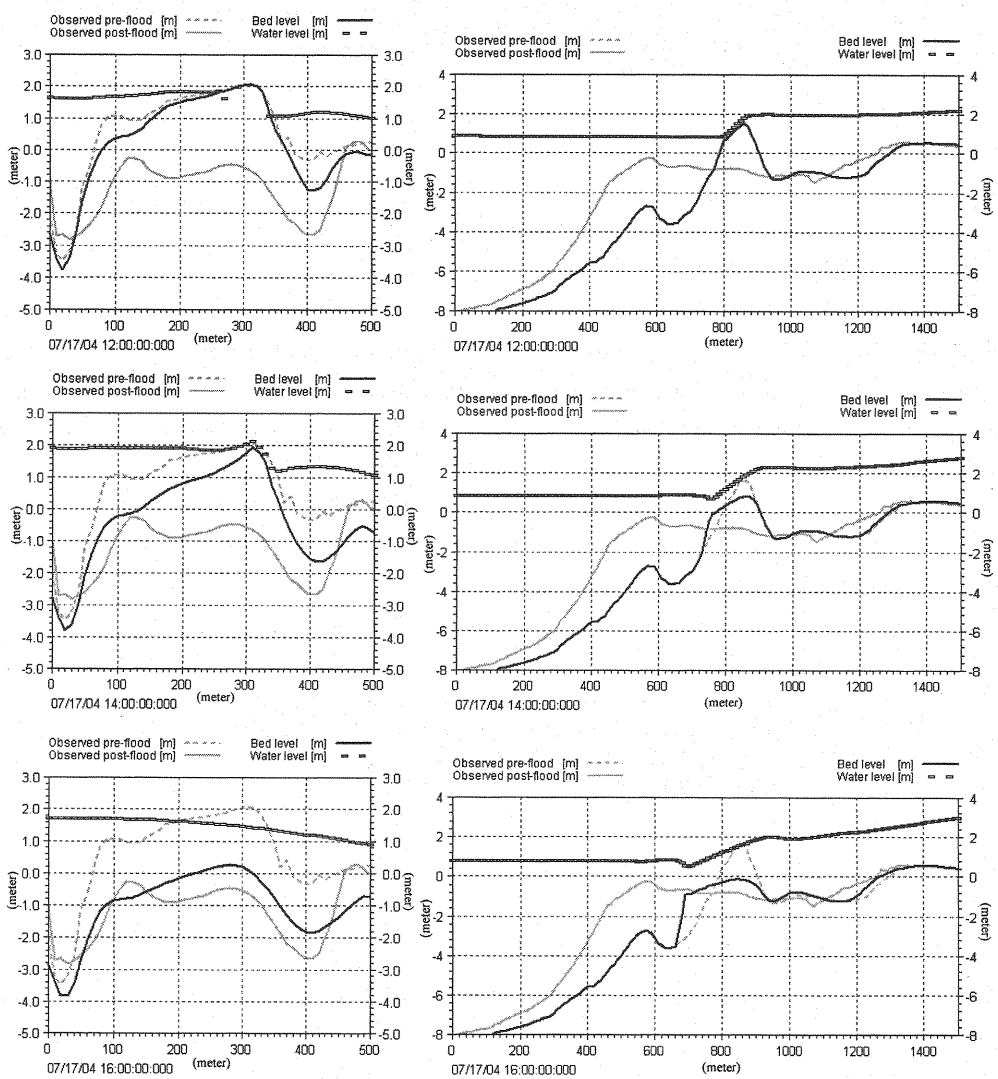

Fig. 9 time series variations of the simulated riverbed and the water level along Line 1 (left) and Line 2 (right).

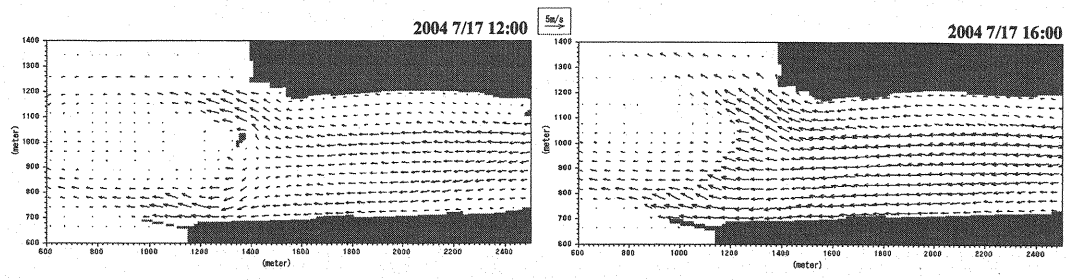

Fig. 10 Distributions of the current speed in the beginning of the flushing (left) and at the peak flow (right).

FACTOR ANALYSIS OF FLUSHING RIVER MOUTH BAR

A factor analysis was conducted to evaluate the influence of discharge, tidal level, and grain size with the calibrated model. First, 3 different peak discharges, 1,600, 3,000, and 4,000 m^3/s, were simulated to examine their influence on a process of flushing. Case1 (1,600m^3/s) corresponds to the flood occurred in Sep. 1999, Case3 (4,000 m^3/s) corresponds to that in July 2004 and Case2 (3,000 m^3/s) corresponds to three-quarters discharge of Case3. In all these cases, the tidal level was set as M.W.L (T.P. +0.34m), other conditions and parameters were the same as that of the calibration case. Fig.11 (left) illustrates simulated cross-sectional bed level profiles of the river mouth bar in post-flood. In these cases, part of the bar remained after the flushing due to a lack of overflow caused by (low) tidal level below the height of the bar (about 2m). This finding indicates that lateral erosion proceeds with increase of the peak discharge and all results reveal similar trends of topographic change. In the event that the increasing rate of discharge exceeds the expansion rate of flow area, water level rises above the bar and overflow occurs resulting in further erosion of the bar.

Fig.11 (right) shows longitudinal profiles with the maximum water level in the simulation. In the case of 3,000 m^3/s and 4,000 m^3/s, the river mouse bar resulted in breakup and then the water level at the upstream of the bar rose up to about 2 m. The water level in case 3 (4,000 m^3/s) was about 0.5m higher than that of case2 (3,000 m^3/s). On the other hand, in case1 (1,600 m^3/s) the water level beside the bar is about 0.5m lower than that of 4,000 m^3/s and about 1.5m lower from the upstream.

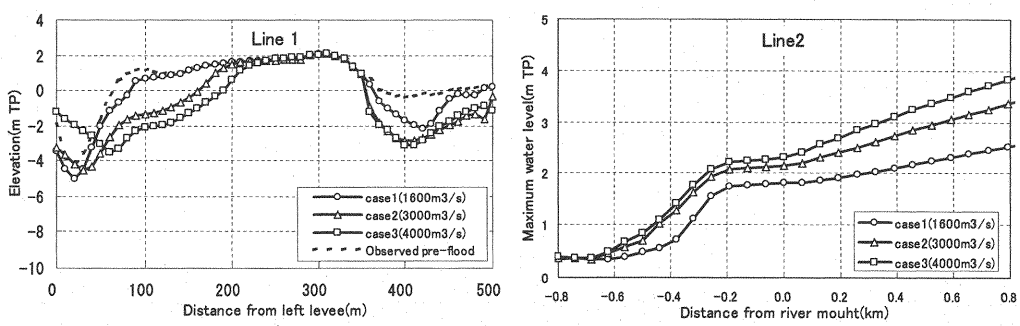

Fig. 11 Comparison of the cross sections (left) and the longitudinal maximum water elevations (right) with various discharges.

To evaluate the effects of the tidal level for flushing the river mouth bar, 4 simulations were conducted: 2 tidal levels (high, low tide) correspond to 2 peak flow (1,600, 4,000 m^3/s). The tide amplitude was set to 1.5 m (T.P.-0.41m to +1.09m). The simulated cross sections of the river mouth bar are plotted in Fig.12 (left). This finding shows that the high tide at the peak flow increases the lateral erosion of the bar more than low tide does. The reason for this is that overflow is subject to high tide at the peak, so that the bar is more eroded. At low tide, on the other hand, the bottom of the channels around the bar tend to become more eroded due to strong currents by steep gradient of the flow, and furthermore expansions of the flow area restrain the occurrence of overflow. Fig.12 (right) shows longitudinal profiles with the maximum water level. In case6 and case7 (4,000 m^3/s), the water level rose up to the height of the bar, and then erosion by the overflow was developed. As a result, water level difference between that of high- and low-tide cases became smaller at the upstream of the bar. On the other hand, in the cases of 1,600 m^3/s, the water level difference at the bar was approximately 0.5m, and it became smaller at the upstream like 4,000 m^3/s cases.

Fig.13 shows the cross sections and the water levels at the peak flow. Bed level change in case4 (1,600 m^3/s), in which the peak flow coincided with high tide, was relatively small. On the other hand, the channels on both sides of the bar were significantly eroded in the case that the peak flow coincided with low tide. At low tide the right side channel became more eroded and the erosion reached almost 1.5m in front of the levee and about 2.5 m in the middle of the channel. The results of different tidal level cases indicate that bed level change around the river mouth bar is much influenced by tidal level during floods. Furthermore, findings reveal that erosion accelerates if the tide is lower than the water level of the channel. Therefore, the effects of tidal level needs to be taken into consideration when designing levees.

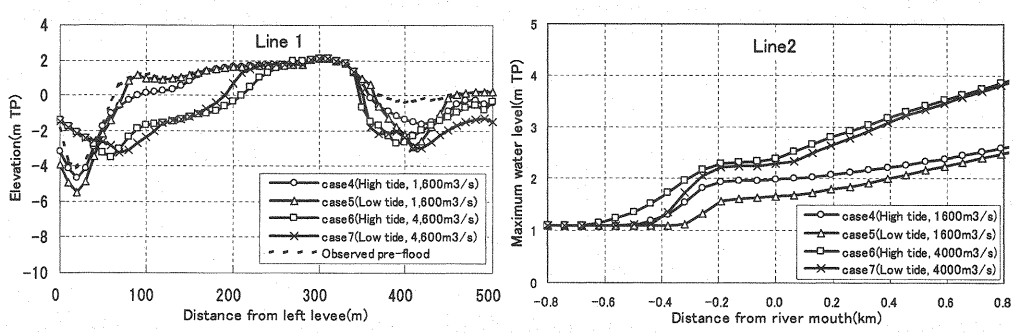

Fig. 12 Comparison of the cross sections (left) and the longitudinal maximum water elevations (right) with various tidal level.

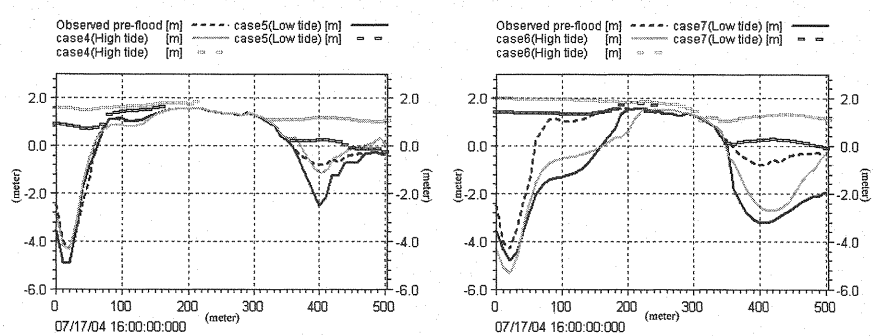

Fig. 13 Comparison of the cross sections and the water level at the peak flow.

Finally, in the next section we examine how the grain size affects a process of the flushing river mouth bar. Fig.14 (left) shows cross sections of the bar simulated with different grain sizes, 0.5 mm, 1.0 mm, 5.0 mm and 22.0 mm, which were based on the bed material survey (See Fig.5). The result shows that the right side of the bar was not flushed out with relatively smaller grain size such as 0.5mm and 1.0mm. On the other hand, the left side became significantly eroded. With larger grain size such as 5mm and 22mm, most of the bar was flushed and the channels on both side of the bar were less eroded as well as the calibration case with 2mm. Furthermore, the amounts of erosion of the bar depend on the grain size. Fig.14 (right) shows simulated longitudinal profiles with the maximum water level for each case. The results indicate that if grain size becomes larger, the water level in the mouth rises. However, the water levels are almost equal at about 1 km upstream from the bar. In contrast, in the case of small grain size, the water level rises only to a small degree due to the erosion of the channels on both sides of the bar at the beginning of flood. However, the water level rises due to that bed level change in the bar and the channel is relatively small at the beginning and it takes time for overflow and flushing to start.

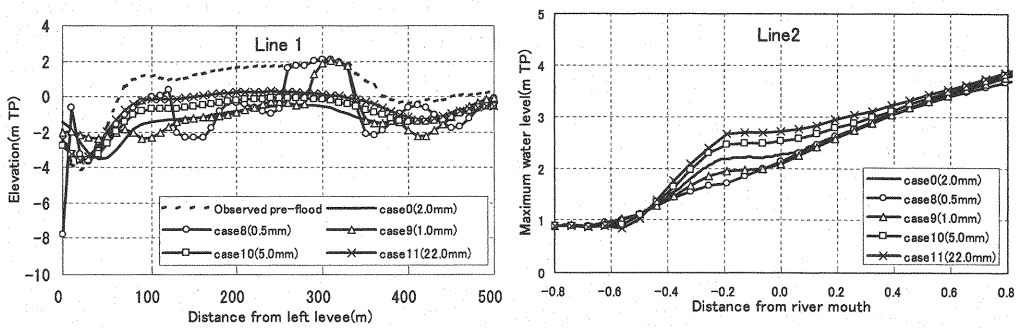

Fig. 14 Comparison of the cross sections (left) and the longitudinal maximum water elevations (right) with various grain size.

CONCLUSION

The simulation of a flushing river mouth bar in the Ara River in July 2004 yielded reliable results in terms of water level fluctuations at the river mouth and topographic change around the bar by making comparisons with the measurements. The findings of our study provide validity of the 2D river morphology model.

As a factor analysis with the calibrated model, the overflow depends on interaction between increase of discharge rate and expansion of flow area at the mouth. Furthermore, the overflow determines the process of flushing river mouse bar. At peak flow with low tide, strong currents erode channels around the bar and they restrain the erosion of the bar. In contrast, the bar is more eroded due to occurrence of overflow at high tide. Moreover, erosion in the channels around the bar tends to accelerate during low tides. Therefore, the effects of tide on topographic change in river mouth need to be considered in channel design.

For the effects of grain size, a bar composed of small grains tends to be flushed partly due to quick progression of the erosion in the channel around the bar. On the other hand, with large grains, the progression is relatively slow and the water level at the upstream rises up. This results in flushing of the whole bar, especially in huge floods, in cases where the bar can be entirely flushed out, a process of the flushing and water level at the upstream of the bar to a great event depend highly on grain size. However, there is less difference in water levels at the upstream far from the bar.

In view of future plans, it is important to improve a simulation accuracy by carrying out field observations of

flushing river mouth bars and to take appropriate measures for the management of river mouth bars, for designing channels, for making sediment control plans in estuaries to control floods, and for dealing with morphological changes in river mouths.

ACKNOWLEDGEMNTS

Prior to this study, valuable measurements and literatures were provided from Uetsu River and National Road Office in Hokuriku Regional Development Bureau, Ministry of Land, Infrastructure and Transport. We hereby express our gratitude to the assistance.

REFFERENCES

1. Chow, V.T. : Open-channel hydraulics, McGraw-Hill, pp.1-680, 1959.
2. Enggrob, H. and Tjerry, S. : Simulation of morphological characteristics of a braided river, IAHR Symposium on river, coastal and estuarine morphodynamics in Genova, 1999.
3. Hosoyamada, T., Sano, Y., Noda, T., Sakai, Y. and Sakawa, H. : A numerical study for flushing of sandbars by flood in the Agano river mouth, Advances in River Engineering, Vol.12, pp.73-78, 2006 (in Japanese).
4. Hosoyamada, T., Tayasu, M., Alwafi, P. and Sato, Y. : Reduction of flood flow capacity due to development of sandbars in river mouth and evaluation of the risk for flood control –a case study for Agano river mouth–, Annual Journal of Hydraulic Engineering, JSCE, Vol.51, pp.967-972, 2007 (in Japanese).
5. Kawaguchi, H., Fukuoka, S. and Abe, T. : Guess of bed variation at the Jouganji river mouth and improvements of river mouth design, Advances in River Engineering, Vol.12, pp.79-84, 2006 (in Japanese).
6. Kuwahara, N., Tanaka, H., Sato, K. and Shuto, N. : Field application of a numerical model for river mouth topography change, Annual Journal of Hydraulic Engineering, JSCE, Vol.40, pp.953-958, 1996 (in Japanese).
7. Olesen, K. W. : Bed topography in shallow river bends, Faculty of Civil Engineering, Delft Univ. of Tech., Report 87-1, 1987.
8. Rozowsky, I. L. : Flow of water in bends of open channels, Academy of Science of the Ukarainian S. S. R., Israel Program for Scientific Translations, pp.1-131, 1957.
9. Sawaragi, T., Deguchi, I., Katakami, T. : Numerical model of deposition shape of river mouth terrace and the effect of river mouth improvement, Proceedings of Coastal Engineering, JSCE, Vol.34, pp.377-381, 1987 (in Japanese).
10. Struiksma, N., Olsen, K. W., Flokstra, C. and de Vriend, H. J. : Bed deformation in curved alluvial channels, Journal of Hydraulic Research, Vol.23, No.1, 1985.
11. Takebayashi, H., Egashira, S., Jin, H. and Sasaki, T. : Temporal change of water level at the upstream side of a river mouth sandbar during floods, Journal of Applied Mechanics, JSCE, Vol.9, pp.997-1006, 2006 (in Japanese).
12. Talmon, A. M. : Bed topography of river bends with suspended sediment transport, Ph.D Thesis, Delft Univ. of Tech., 1992.
13. Van Rijn, L. C. : Part I: Bed load transport, Journal of Hydraulic Engineering, Vol.110, No.10, pp.1431-1456, October 1984.
14. Van Rijn, L. C. : PartII: Suspended load transport, Journal of Hydraulic Engineering, Vol.110, No.11, pp.1613-1641,

November 1984.

15. Watanabe, K., Nguyen, T. and Tanaka, H. : Field observations of sand spit flushing and its recovery at the Natori river mouth, Proceedings of Coastal Engineering, JSCE, Vol.52, pp.586-590, 2005 (in Japanese).

APPENDIX - NOTATION

The following symbols are used in this paper:

a = calibration coefficient in the bank erosion model;
b = calibration coefficient in the bank erosion model;
c_a = reference concentration ;
C = Chezy number;
d_{50} = median diameter of the sediment;
D_* = dimensionless particle parameter in Van Rijn's model;
E = eddy viscosity;
E_b = bank erosion rate;
f = correction factor for suspended load
g = gravity acceleration;
G = transverse bed slope factor;
h = water depth;
H = water level;
M = Manning's roughness coefficient;
n = horizontal coordinate in a transverse direction;
p = mass fluxes in the s-direction;
q = mass fluxes in the n-direction;
q_s = near bank sediment transport;
r = relative density of the sediment;
RHS_n = right hand side in the force balance in the n- direction
RHS_s = right hand side in the force balance in the s-direction
R_n = radius of curvature of n-line;
R_s = radius of curvature of s-line;
s = horizontal coordinate along the streamline;
S_{bl} = bed load sediment transport rate;
S_{bn} = bed load sediment transport rate in the n- direction;
S_{bs} = bed load sediment transport rate in the s-direction;
S_n = total sediment transport in the n- direction;
S_s = total sediment transport in the s- direction;
S_{sl} = suspended load transport rate
T = transport stage parameter Van Rijn's model;

$\tan\delta_s$ = bed shear direction change due to helical flow strength;

u = velocity component in the s-direction;

v = velocity component in the n-direction;

V = volume of lateral erosion;

z = bed level;

α = correction coefficient for the bed slope effect;

Δn = transverse length of the cell calibration coefficient;

Δs = longitudinal length of the cell;

ΔS_e = lateral sediment supply from bank erosion;

γ = transverse bed slope exponent;

κ_{sf} = length scale for secondary flow adaptation;

λ = sediment porosity; and

θ = Shields parameter.

(Received Jul 09, 2007 ; revised Nov 01, 2007)